Advances in Applied Mathematics and Mechanics
Adv. Appl. Math. Mech., Vol. **11**, No. 3, pp. 598-607

DOI: 10.4208/aamm.2018.s04
June 2019

On the Comparison Between Lattice Boltzmann Methods and Spectral Methods for DNS of Incompressible Turbulent Channel Flows on Small Domain Size

Liren Li[1], Yipeng Shi[1], Shengqi Zhang[1], Lian-Ping Wang[2] and Zhenhua Xia[3,*]

[1] *State Key Laboratory for Turbulence and Complex Systems, College of Engineering, Peking University, Beijing 100871, China*
[2] *Department of Mechanics and Aerospace Engineering, Southern University of Science and Technology, Shenzhen 518055, Guangdong, China*
[3] *Department of Engineering Mechanics, Zhejiang University, Hangzhou 310027, Zhejiang, China*

Received 19 August 2018; Accepted (in revised version) 6 December 2018

Abstract. The paper presents a study of the influence of the domain size and LBM collision models on fully developed turbulent channel flows. The results using spectral method show that a smaller domain size will increase the velocity fluctuations in the streamwise direction. And MRT-LBM with different collision models gives reliable results at least for low order flow statistics compared with those from spectral method and finite-difference method.

AMS subject classifications: 76F65, 76M28

Key words: Lattice Boltzmann method, Spectral method, turbulent channel flows.

1 Introduction

Over the last 30 years, direct numerical simulations (DNS) have been applied to investigate a large number of turbulent flows, which generates more details about the mechanisms of turbulent transport than experimental methods. For simple geometries, many algorithms have been applied to simulate turbulence, e.g., finite-difference method, pseudo-spectral method and Lattice Boltzmann Method (LBM). Pseudo-spectral method is considered to be the most reliable method for its high-order spatial accuracy and low numerical dissipation when compared at the same temporal and spatial resolutions

*Corresponding author.
Email: xiazh@zju.edu.cn (Z. H. Xia)

with alternative methods. However, when the geometries are complex, finite-difference method and pseudo-spectral method are difficult to be used. A fully mesoscopic LBM as an alternative approach to incompressible turbulence is easy to deal with complex geometries and easy to parallelize. This offers the potential for the LBM to be applied to treat turbulent particle-laden flows.

Fully developed incompressible turbulent channel flows are considered here. The benchmark Navier-Stokes solutions simulated by Chebyshev pseudo-spectral method KMM [1] are used as a comparison. Lammers et al. [2] reviewed the former studies of LBM DNS on developed channel flows and also used a BGK (single-relaxation-time) D3Q19 model to simulate the channel flow turbulence which is in great agreement with the result of KMM. Suga [3] used a MRT(multiple-relaxation-time) D3Q27 model and also obtained good results. Freitas [4] performed a comparative study of different discretizations, i.e., D3Q19 and D3Q27 model, applied to a turbulent channel flow at $Re_\tau = 200$. Averaged streamwise velocity and rms(root-mean-squared) velocity are reasonable for both D3Q19 and D3Q27. However, the peak of the streamwise component of the Reynolds stress is more accurately predicted by the D3Q27 model. Kang and Hassan [5] reported that the D3Q19 model breaks the rotational invariance and produces unphysical results especially for turbulent wall-bounded flows–turbulent circular pipe and square duct flows, while the D3Q27 model achieves the rotational invariance. Thus, we use the D3Q27 model in this paper.

Gehrke et al. [6] reported the potential influence of the collision models in LBM, i.e., the BGK, the MRT and the Cumulant model on DNS of turbulent channel flows. The BGK model is the single-relaxation-time model, which is simple and often become unstable when the Reynolds number is high. Then multiple-relaxation-time (MRT) model is proposed by d'Humieres [7] to overcome this difficulties. MRT model allows each physical process to have its own relaxation time in order to improve the numerical stability and physical accuracy. The results show that the mean velocity profiles of the MRT and the Cumulant model are slightly higher than the BGK model and KMM. Wang et al. [8] used LBM and Yu et al. [9] used finite-difference method to study a smaller domain size ($4H \times 2H \times 2H$) turbulent channel flows. Yu also obtained a higher mean velocity profile and they both found a higher rms velocity in the streamwise direction. We will use the pseudo-spectral method to show the influence of the domain size in Section 3.1 and compare the different LBM-MRT D3Q27 models on small domain size ($4H \times 2H \times 2H$) in Section 3.2.

2 Numerical methods

2.1 Lattice Boltzmann method

We use the MRT-LBE collision model with Q discrete velocities in three dimensions. The evolution equation for the MRT-LBE on each lattice node $\mathbf{x}$ at time t can be written as the

following:

$$\mathbf{f}(\mathbf{x}+\mathbf{c}\delta t,t+\delta t)=\mathbf{f}(\mathbf{x},t)-\mathbf{M}^{-1}\mathbf{S}[\mathbf{m}-\mathbf{m}^{(eq)}]+\mathbf{F}, \tag{2.1}$$

where the $Q\times Q$ matrix $\mathbf{M}$ transforms the discrete particle density distribution functions $\mathbf{f}\in\mathbb{V}=\mathbb{R}^Q$ to the velocity moments $\mathbf{m}\in\mathbb{M}=\mathbb{R}^Q$:

$$\mathbf{m}=\mathbf{M}\cdot\mathbf{f},\quad \mathbf{f}=\mathbf{M}^{-1}\cdot\mathbf{m}, \tag{2.2}$$

which means the collision is performed in the moment space $\mathbb{M}$, while the streaming is executed in the velocity space $\mathbb{V}$ and $\mathbf{F}$ represents an external body force.

For $Q=27$, the D3Q27 model includes discrete velocities vectors read

$$c_i=\begin{cases}(0,0,0), & i=0,\\ c(\pm1,0,0),c(0,\pm1,0),c(0,0,\pm1), & i=1,2,\cdots,6,\\ c(\pm1,\pm1,0),c(\pm1,0,\pm1),c(0,\pm1,\pm1), & i=7,8,\cdots,18,\\ c(\pm1,\pm1,\pm1), & i=19,20,\cdots,26,\end{cases} \tag{2.3}$$

where $c=\delta x/\delta t$.The corresponding moments for D3Q27 are the corresponding 27 moments for D3Q27 model are

$$\begin{aligned}\mathbf{m}_{27}=&(\delta\rho,j_x,j_y,j_z,e,p_{xx},p_{zz},p_{xy},p_{yz},p_{xz},q_x,q_y,q_z,\pi_x,\\ &\pi_y,\pi_z,\phi_{xyz},\epsilon,\psi_{xx},\psi_{zz},\psi_{xy},\psi_{yz},\psi_{xz},\xi_x,\xi_y,\xi_z,e^3)^\dagger.\end{aligned} \tag{2.4}$$

The details of the corresponding equilibrium moments could be found in Appendix. The density ρ could be decomposed into the mean density ρ_0 and the density fluctuation $\delta\rho$. We use $\delta\rho$ instead of ρ in the LBE simulations, for it is more accurate for the incompressible flows [10]

$$\rho=\rho_0+\delta\rho,\quad \rho_0=1. \tag{2.5}$$

The relaxation matrix S is diagonal and each of diagonal elements means the corresponding moment relaxation rate. MRT-LBE model individually control the different moments' relaxation to achieve better accuracy and stability. If we simply set all of the relaxation rates to be a single value s_ν, i.e., $S=s_\nu I$, then the model will be reduced to the BGK model. The D3Q27 MRT relaxation matrix S_{27} is

$$\begin{aligned}\mathbf{S}_{27}=&diag(0,0,0,0,s_e,s_\nu,s_\nu,s_\nu,s_\nu,s_\nu,s_q,s_q,s_q,s_\pi,\\ &s_\pi,s_\pi,s_\phi,s_\epsilon,s_\psi,s_\psi,s_\psi,s_\psi,s_\psi,s_\xi,s_\xi,s_\xi,s_{e^3}).\end{aligned} \tag{2.6}$$

Through the Chapman-Enskog analysis of the MRT model we could recover a macroscopic Navier-Stokes equaiton. Unlike in the LBGK model, the shear viscosity ν and the bulk viscosity ζ can be chosen independently

$$\nu=\frac{1}{3}\Big(\frac{1}{s_\nu}-\frac{1}{2}\Big)\delta t, \tag{2.7a}$$

$$\zeta=\frac{5-9c_s^2}{9}\Big(\frac{1}{s_e}-\frac{1}{2}\Big)\delta t. \tag{2.7b}$$

Table 1: parameters settings for different collision models.

Label	s_e	s_ϵ	s_q	s_ν	s_π	s_ϕ	s_ψ	s_ξ	s_{e^3}
BGK27	s_ν	s_ν	s_ν	$\frac{\delta t}{3\nu+0.5\delta t}$	s_ν	s_ν	s_ν	s_ν	s_ν
MRT27suga [3]	1.54	1.4	1.5	$\frac{\delta t}{3\nu+0.5\delta t}$	1.74	1.4	1.98	1.83	1.61
MRT27LD	1.8	1.8	1.8	$\frac{\delta t}{3\nu+0.5\delta t}$	1.8	1.8	1.8	1.8	1.8

And different collision models are shown in Table 1. s_ν and s_e are the relaxation time for the second order tensors and the kinetic energy, respectively. The stability condition needs all the relaxation parameters satisfy $0<s_i<2$. Lallemand and Luo [11] pointed out that the other relaxation parameters only have effects on higher order terms, which do not influence the transport coefficients, i.e., shear viscosity ν and bulk viscosity ζ. Suga [3] gives a set of optimized relaxation parameters called MRT27suga in Table 1. Wang [8] intends to minimize the numerical dissipation by using a smaller bulk viscosity, called MRT27LD (low dissipation). It should be noted that BGK model is much more unstable than MRT27suga and MRT27LD when simulating the particle-laden turbulent flows. But, for the given resolution, the BGK model is also stable in our single-phase turbulence simulations.

2.2 Finite difference method

Our LBM results are mainly compared with results from pseudo-spectral method used by Kim [1] and finite-difference method used by Yu [9]. Here, we briefly introduce the main idea of the finite-difference method used by Yu. The Naiver-Stokes equations are solved with a finite-difference-based projection method on a homogeneous half-stagger grid. Spatial derivatives are discretized with the second-order central difference scheme. That means the grids are uniform in all directions in Yu's method like the LBM, while non-uniform meshes are used in the normal direction in pseudo-spectral method. The non-uniform normal direction meshes used in the spectral method are $y_j=\cos(j-1)\pi/(N-1)$, $j=1,2,\cdots,N$. For $N=129$ in KMM, the minimum spacing is the first grid near the wall at $y^+\simeq 0.05$ and the maximum spacing is $\Delta y^+\simeq 4.4$ at the centerline of the channel, which is larger than the uniform spacing of LBM and Yu's finite-difference method. To minimize the influence of the maximum spacing in the normal direction, we conduct the case Sp422fine whose domain size is $4H\times 2H\times 2H$ and maximum spacing is $\Delta y^+\simeq 2.9$.

3 Results

We consider a fully developed turbulent channel flow with x, y and z representing the streamwise, normal and spanwise directions, respectively. The domain size is $L_x\times 2H\times L_z$. The turbulent flow is driven by constant pressure gradient in the x direction, which is modeled by a constant body force. The frictional Reynolds number is defined as $Re_\tau=$

$u_\tau H/\nu = 180$ in our simulations, where ν is the kinematic viscosity and $u_\tau = \sqrt{\tau_w/\rho}$ is the frictional velocity. At the fully developed stage, the wall viscous shear stress τ_w should be balanced with body force (pressure gradient) $2\tau_w L_x L_z = \rho g 2HL_x L_z$, where ρ is the fluid density and g is the body force per unit mass. Period boundary condition is assumed in the streamwise x and spanwise z directions and no-slip condition on the two channel walls using halfway bounce-back method.

3.1 Domain size

We use spectral methods to investigate the influence of domain size on turbulent channel flows. The grid parameters of three simulations for turbulent channel flows are shown in Table 2, compared with the reference database [1]. Due to the argument that the grid sizes of the streamwise and spanwise directions are too wide compared with the normal direction in the KMM simulation, we perform the simulation with even smaller grid sizes in the streamwise and spanwise directions called Sp422fine.

First, we illustrate that even the grid sizes in the streamwise and spanwise directions are large in the KMM and Sp422coarse, but the mean velocity profiles on a log-linear plot displayed in Fig. 1(a) and the rms(root-mean-squared) velocity profiles displayed in Fig. 1(b) show that Sp422coarse and Sp422fine give the same results. However, the rms velocity profiles (Fig. 1(b)) show a larger streamwise rms velocity and smaller spanwise rms velocity in the Sp422fine and Sp422coarse simulations for the smaller domain sizes ($4H\times 2H\times 2H$) than those of KMM for the domain sizes ($4\pi H\times 2H\times 2\pi H$). So the domain sizes influence the turbulence statistics.

Next, we compare four different domain sizes, i.e., Sp422fine, Sp623, KMM and Sp824. Each domain size is larger than the previous one. The mean velocity profiles on a log-linear plot are shown in Fig. 2(a). The result shows the influence of the domain size does not change the mean velocity profiles. Four simulations fit well with each other. The peak of the streamwise rms velocity changes a lot in different domain sizes shown in Fig. 2(b). When the domain size is smaller, the peak of the streamwise rms velocity is larger. The peak of the spanwise rms velocity is opposite. The domain size is smaller, the peak of the spanwise rms velocity is smaller too. And the normal rms velocity does not seem to change with the domain sizes. The reason why the streamwise velocity is strengthened is that with the domain size decreasing the coherence of the structure in the streamwise

Table 2: Spectral method parameters settings for turbulent channel flows.

Run	Domain size	$N_x\times N_y\times N_z$	Re_τ	$\Delta y^+_{\max}$	Δx^+	Δz^+
KMM	$4\pi H\times 2H\times 2\pi H$	$192\times 129\times 160$	180	4.4	11.8	7
Sp824	$8\pi H\times 2H\times 4\pi H$	$384\times 193\times 384$	180	2.9	11.8	5.9
Sp623	$6H\times 2H\times 3H$	$576\times 193\times 288$	180	2.9	1.9	1.9
Sp422fine	$4H\times 2H\times 2H$	$384\times 193\times 192$	180	2.9	1.9	1.9
Sp422coarse	$4H\times 2H\times 2H$	$72\times 193\times 72$	180	2.9	10	5

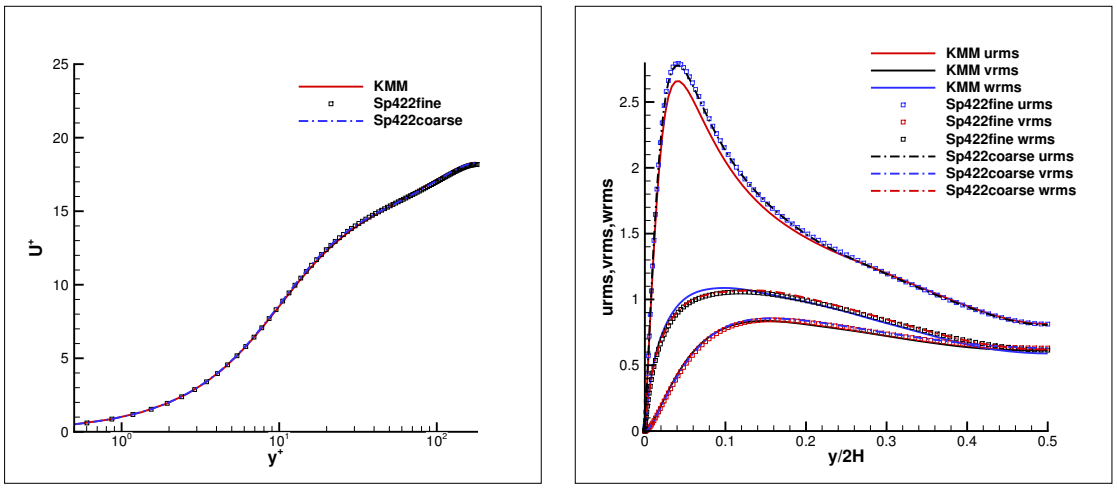

(a) (b)

Figure 1: (a) mean velocity profiles Sp422coarse vs Sp422fine; (b) RMS velocity profiles.

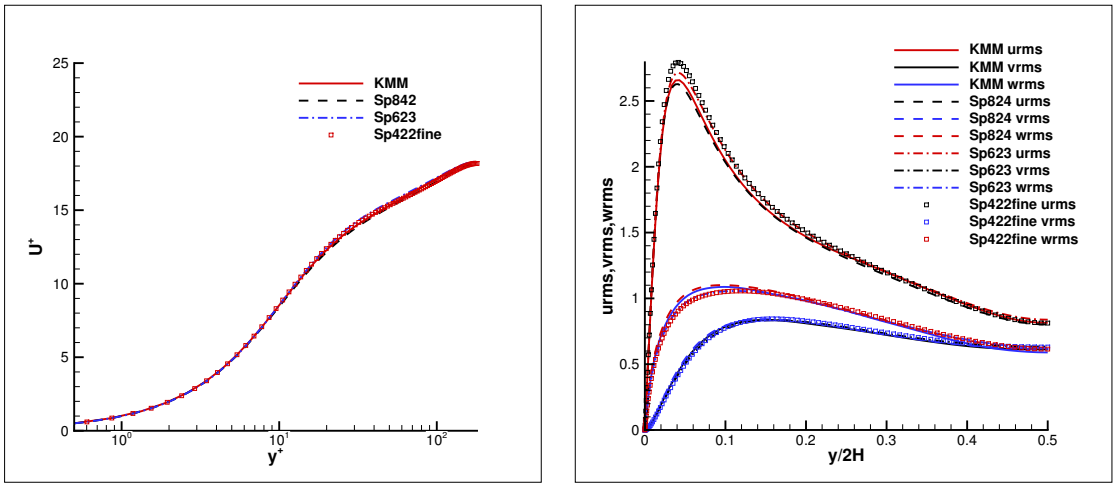

(a) (b)

Figure 2: (a) mean velocity profiles in four different domain sizes; (b) RMS velocity profiles.

direction is enhanced.

3.2 LBM models

Next, we use lattice Boltzmann method to simulate the same domain size with Sp422fine in Section 3.1. Three different MRT models as shown in Table 1 are compared with Yu's

Table 3: LBM parameters settings for turbulent channel flows.

Run	Domain size	$N_x \times N_y \times N_z$	Re_τ	$\Delta y^+_{\max}$	Δx^+	Δz^+
SP422fine	$4H \times 2H \times 2H$	$384 \times 193 \times 192$	180	2.9	1.9	1.9
LBM27BGK	$4H \times 2H \times 2H$	$400 \times 200 \times 200$	180	1.8	1.8	1.8
LBM27suga	$4H \times 2H \times 2H$	$400 \times 200 \times 200$	180	1.8	1.8	1.8
LBM27LD	$4H \times 2H \times 2H$	$400 \times 200 \times 200$	180	1.8	1.8	1.8
Yu	$4H \times 2H \times 2H$	$256 \times 128 \times 128$	180	2.8	2.8	2.8

finite different method and spectral method Sp422fine. Details are displayed in Table 3. The grid resolution is quantified by the value of $\Delta y^+ = 1.8$, which Lammer [2] suggested that this value should be less than 2.25 using BGK model. Note that the grid size of LBM is much smaller than that of the spcetral method in the direction normal to the wall at $y^+ > 12$.

The mean velocity profiles and relative difference with Sp422fine are displayed in Fig. 3(a). LBM with different collision models gives almost the same velocity profiles and rms velocity profiles. When the result is stable, the influence of different collision models seem to be negligible. The LBM's and Yu's results are in great agreement which are slightly larger than spectral method's result Sp422fine at $y^+ > 12$. The rms (root-mean-squared) velocity profiles (Fig. 3(b)) fit well with Yu's and Sp422fine's results. The reason why the LBM's and Yu's results are slightly higher may be because the grid size of the normal direction is uniform while that of the spectral method is not. On the condition that all the methods have resolved the small-scale structures near the wall, a uniform grid in all three directions near the center of the channel guarantees the nearly isotropic

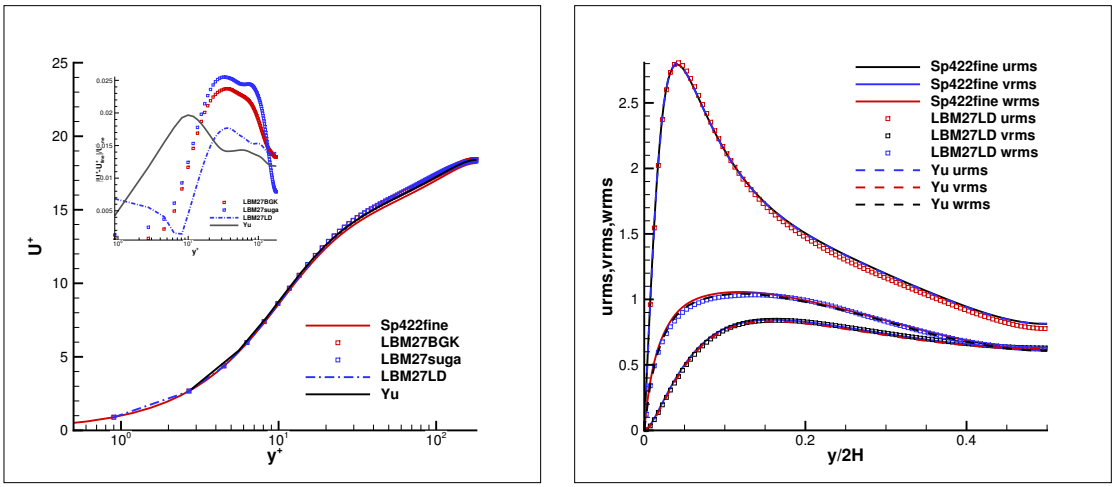

(a) (b)

Figure 3: (a) mean velocity profiles and their relative difference with Sp422fine; (b) RMS velocity profiles.

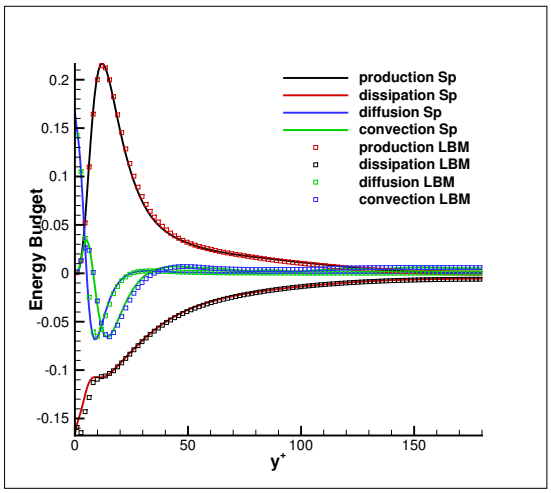

Figure 4: Budget terms of the turbulent kinetic energy Sp422fine vs MRT27LD.

turbulence away from the wall. Fig. 4 also shows the comparison of the budget terms of the turbulent kinetic energy between Sp422fine and MRT27LD. It is seen that each agreement between the spectral method and the D3Q27 MRT-LBM is almost perfect. Thus, it is confirmed that the LBM is as reliable as the spectral method for DNSs of turbulent channel flows on small domain size.

4 Conclusions

An accurate prediction of fully developed turbulent channel flows by LBM is shown compared with the pseudo-spectral method on small domain size. Both LBM and spectral methods show that the shortened streamwise and spanwise domain sizes will lead to larger fluctuations in the streamwise direction. Different LBM collision models yield almost the same mean velocity profiles and rms velocity, which agree well with finite-difference method Yu's results. However, both LBM and Yu's mean velocity profiles are slightly higher than that from the spectral methods.

Appendix: details of the employed D3Q27 MRT model

The D3Q27 model [12] consists of one zero-order moment $\delta\rho$, three first-order moments j_x, j_y, j_z, six second-order moments e, p_{xx}, p_{zz}, p_{xy}, p_{yz}, p_{xz}, seven third-order moments q_x, q_y, q_z, π_x, π_y, π_z, ϕ_{xyz}, six fourth-order moments ϵ, ψ_{xx}, ψ_{zz}, ψ_{xy}, ψ_{yz}, ψ_{xz}, three fifth-order moments ξ_x, ξ_y, ξ_z and one sixth-order moments e^3

$$\delta\rho=\sum_{\alpha=0}^{26}f_\alpha, \tag{A.1a}$$

$$j_x=\sum_{\alpha=0}^{26}f_\alpha e_{\alpha x},\quad j_y=\sum_{\alpha=0}^{26}f_\alpha e_{\alpha y},\quad j_z=\sum_{\alpha=0}^{26}f_\alpha e_{\alpha z}, \tag{A.1b}$$

$$e=\sum_{\alpha=0}^{26}f_\alpha(e_{\alpha x}^2+e_{\alpha y}^2+e_{\alpha z}^2), \tag{A.1c}$$

$$p_{xx}=\sum_{\alpha=0}^{26}f_\alpha(2e_{\alpha x}^2-e_{\alpha y}^2-e_{\alpha z}^2),\quad p_{zz}=\sum_{\alpha=0}^{26}f_\alpha(e_{\alpha y}^2-e_{\alpha z}^2), \tag{A.1d}$$

$$p_{xy}=\sum_{\alpha=0}^{26}f_\alpha(e_{\alpha x}e_{\alpha y}),\quad p_{yz}=\sum_{\alpha=0}^{26}f_\alpha(e_{\alpha y}e_{\alpha z}),\quad p_{xz}=\sum_{\alpha=0}^{26}f_\alpha(e_{\alpha x}e_{\alpha z}), \tag{A.1e}$$

$$q_x=\sum_{\alpha=0}^{26}f_\alpha(e_{\alpha x}^2+e_{\alpha y}^2+e_{\alpha z}^2)e_{\alpha x},\quad q_y=\sum_{\alpha=0}^{26}f_\alpha(e_{\alpha x}^2+e_{\alpha y}^2+e_{\alpha z}^2)e_{\alpha y}, \tag{A.1f}$$

$$q_z=\sum_{\alpha=0}^{26}f_\alpha(e_{\alpha x}^2+e_{\alpha y}^2+e_{\alpha z}^2)e_{\alpha z}, \tag{A.1g}$$

$$\pi_x=\sum_{\alpha=0}^{26}f_\alpha(e_{\alpha y}^2-e_{\alpha z}^2)e_{\alpha x},\quad \pi_y=\sum_{\alpha=0}^{26}f_\alpha(e_{\alpha z}^2-e_{\alpha x}^2)e_{\alpha y},\quad \pi_z=\sum_{\alpha=0}^{26}f_\alpha(e_{\alpha x}^2-e_{\alpha y}^2)e_{\alpha z}, \tag{A.1h}$$

$$\phi_{xyz}=\sum_{\alpha=0}^{26}f_\alpha(e_{\alpha x}e_{\alpha y}e_{\alpha z}),\quad \epsilon=\sum_{\alpha=0}^{26}f_\alpha(e_{\alpha x}^2+e_{\alpha y}^2+e_{\alpha z}^2)^2, \tag{A.1i}$$

$$\psi_{xx}=\sum_{\alpha=0}^{26}f_\alpha(2e_{\alpha x}^2-e_{\alpha y}^2-e_{\alpha z}^2)(e_{\alpha x}^2+e_{\alpha y}^2+e_{\alpha z}^2),\quad \psi_{zz}=\sum_{\alpha=0}^{26}f_\alpha(e_{\alpha y}^2-e_{\alpha z}^2)(e_{\alpha x}^2+e_{\alpha y}^2+e_{\alpha z}^2), \tag{A.1j}$$

$$\psi_{xy}=\sum_{\alpha=0}^{26}f_\alpha(e_{\alpha x}e_{\alpha y})(e_{\alpha x}^2+e_{\alpha y}^2+e_{\alpha z}^2),\quad \psi_{yz}=\sum_{\alpha=0}^{26}f_\alpha(e_{\alpha y}e_{\alpha z})(e_{\alpha x}^2+e_{\alpha y}^2+e_{\alpha z}^2), \tag{A.1k}$$

$$\psi_{xz}=\sum_{\alpha=0}^{26}f_\alpha(e_{\alpha x}e_{\alpha z})(e_{\alpha x}^2+e_{\alpha y}^2+e_{\alpha z}^2),\quad \xi_x=\sum_{\alpha=0}^{26}f_\alpha(e_{\alpha x}^2+e_{\alpha y}^2+e_{\alpha z}^2)^2e_{\alpha x}, \tag{A.1l}$$

$$\xi_y=\sum_{\alpha=0}^{26}f_\alpha(e_{\alpha x}^2+e_{\alpha y}^2+e_{\alpha z}^2)^2e_{\alpha y},\quad \xi_z=\sum_{\alpha=0}^{26}f_\alpha(e_{\alpha x}^2+e_{\alpha y}^2+e_{\alpha z}^2)^2e_{\alpha z}, \tag{A.1m}$$

$$e^3=\sum_{\alpha=0}^{26}f_\alpha(e_{\alpha x}^2+e_{\alpha y}^2+e_{\alpha z}^2)^3. \tag{A.1n}$$

Acknowledgements

This work was supported by the National Science Foundation of China (NSFC grant Nos. 91852205 and 91752202). The author would like to thank the referees for the helpful suggestions.

References

[1] J. KIM, P. MOIN AND R. MOSER, *Turbulence statistics in fully developed channel flow at low Reynolds number,* J. Fluid Mech., 177 (1987), pp. 136–166.

[2] P. LAMMERS AND K. N. BERONOV, R. VOLKERT, G. BRENNER AND F. DURST, *Lattice BGK direct numerical simulation of fully developed turbulence in incompressible plane channel flow,* Comput. Fluids, 35 (2006), pp. 1137–1153.

[3] K. SUGA, Y. KUWATA, K. TAKASHIMA AND R. CHIKASUE, *A D3Q27 multiple-relaxation-time lattice Boltzmann method for turbulent flows,* Comput. Math. Appl., 69 (2015), pp. 518–529.

[4] K. RAINHILL FREITAS, ANDREAS HENZE, MATTHIAS MEINKE AND WOLFGANG SCHRDER, *Analysis of Lattice-Boltzmann methods for internal flows,* Comput. Fluids, 47 (2011), pp. 115–121.

[5] SHIN K. KANG AND YASSIN A. HASSAN, *The effect of lattice models within the lattice Boltzmann method in the simulation of wall-bounded turbulent flows,* J. Comput. Phys., 232 (2013), pp. 100–117.

[6] M. GEHRKE AND C. F. JANEN AND T. RUNG, *Scrutinizing lattice Boltzmann methods for direct numerical simulations of turbulent channel flows,* Comput. Fluids, 156 (2017), pp. 247–263.

[7] P. V. COVENEY, S. SUCCI, D'HUMIÈRES DOMINIQUE, IRINA GINZBURG, MANFRED KRAFCZYK, PIERRE LALLEMAND AND LISHI LUO, *Multiple relaxation time lattice Boltzmann models in three dimensions,* The Royal Society, 360 (2002), pp. 437–451.

[8] LIANPING WANG, CHENG PENG, ZHAOLI GUO AND ZHAOSHENG YU, *Lattice Boltzmann simulation of particle-laden turbulent channel flow,* Comput. Fluids, 124 (2016), pp. 226–236.

[9] X. M. SHAO, T. H. WU AND Z. S. YU, *Fully resolved numerical simulation of particle-laden turbulent flow in a horizontal channel at a low Reynolds number,* J. Fluid Mech., 693 (2012), pp. 319–344.

[10] X. Y. HE AND L. S. LUO, *Lattice Boltzmann model for the incompressible Navier–Stokes equation,* J. Statistical Phys., 88 (1997), pp. 927–944.

[11] LALLEMAND PIERRE AND L. S. LUO, *Theory of the lattice Boltzmann method: Dispersion, dissipation, isotropy, Galilean invariance and stability,* Phys. Rev. E, 61 (2000), 6546.

[12] HARISH OPADRISHTA, Multiple-Relaxation-Time Lattice Boltzmann Simulations of Turbulent Channel and Pipe Flow, thesis, 2016.